Diffractive Hard Photoproduction at HERA and Evidence for the Gluon Content of the Pomeron

ZEUS Collaboration

Abstract

Inclusive jet cross sections for events with a large rapidity gap with respect to the proton direction from the reaction $ep \rightarrow jet + X$ with quasi-real photons have been measured with the ZEUS detector. The cross sections refer to jets with transverse energies $E_T^{jet} > 8$ GeV. The data show the characteristics of a diffractive process mediated by pomeron exchange. Assuming that the events are due to the exchange of a pomeron with partonic structure, the quark and gluon content of the pomeron is probed at a scale $\sim (E_T^{jet})^2$. A comparison of the measurements with model predictions based on QCD plus Regge phenomenology requires a contribution of partons with a hard momentum density in the pomeron. A combined analysis of the jet cross sections and recent ZEUS measurements of the diffractive structure function in deep inelastic scattering gives the first experimental evidence for the gluon content of the pomeron in diffractive hard scattering processes. The data indicate that between 30% and 80% of the momentum of the pomeron carried by partons is due to hard gluons.

The ZEUS Collaboration

M. Derrick, D. Krakauer, S. Magill, D. Mikunas, B. Musgrave, J. Repond, R. Stanek, R.L. Talaga, H. Zhang
Argonne National Laboratory, Argonne, IL, USA [p]

R. Ayad[1], G. Bari, M. Basile, L. Bellagamba, D. Boscherini, A. Bruni, G. Bruni, P. Bruni, G. Cara Romeo,
G. Castellini[2], M. Chiarini, L. Cifarelli[3], F. Cindolo, A. Contin, M. Corradi, I. Gialas[4], P. Giusti, G. Iacobucci,
G. Laurenti, G. Levi, A. Margotti, T. Massam, R. Nania, C. Nemoz,
F. Palmonari, A. Polini, G. Sartorelli, R. Timellini, Y. Zamora Garcia[1], A. Zichichi
University and INFN Bologna, Bologna, Italy [f]

A. Bargende[5], J. Crittenden, K. Desch, B. Diekmann[6], T. Doeker, M. Eckert, L. Feld, A. Frey, M. Geerts,
M. Grothe, H. Hartmann, K. Heinloth, E. Hilger, H.-P. Jakob, U.F. Katz, S.M. Mari[4], S. Mengel, J. Mollen,
E. Paul, M. Pfeiffer, Ch. Rembser, D. Schramm, J. Stamm, R. Wedemeyer
Physikalisches Institut der Universität Bonn, Bonn, Federal Republic of Germany [c]

S. Campbell-Robson, A. Cassidy, N. Dyce, B. Foster, S. George, R. Gilmore, G.P. Heath, H.F. Heath, T.J. Llewellyn,
C.J.S. Morgado, D.J.P. Norman, J.A. O'Mara, R.J. Tapper, S.S. Wilson, R. Yoshida
H.H. Wills Physics Laboratory, University of Bristol, Bristol, U.K. [o]

R.R. Rau
Brookhaven National Laboratory, Upton, L.I., USA [p]

M. Arneodo[7], M. Capua, A. Garfagnini, L. Iannotti, M. Schioppa, G. Susinno
Calabria University, Physics Dept.and INFN, Cosenza, Italy [f]

A. Bernstein, A. Caldwell, N. Cartiglia, J.A. Parsons, S. Ritz[8], F. Sciulli, P.B. Straub, L. Wai, S. Yang, Q. Zhu
Columbia University, Nevis Labs., Irvington on Hudson, N.Y., USA [q]

P. Borzemski, J. Chwastowski, A. Eskreys, K. Piotrzkowski, M. Zachara, L. Zawiejski
Inst. of Nuclear Physics, Cracow, Poland [j]

L. Adamczyk, B. Bednarek, K. Jeleń, D. Kisielewska, T. Kowalski, E. Rulikowska-Zarębska,
L. Suszycki, J. Zając
Faculty of Physics and Nuclear Techniques, Academy of Mining and Metallurgy, Cracow, Poland [j]

A. Kotański, M. Przybycień
Jagellonian Univ., Dept. of Physics, Cracow, Poland [k]

L.A.T. Bauerdick, U. Behrens, H. Beier[9], J.K. Bienlein, C. Coldewey, O. Deppe, K. Desler, G. Drews,
M. Flasiński[10], D.J. Gilkinson, C. Glasman, P. Göttlicher, J. Große-Knetter, B. Gutjahr[11], T. Haas, W. Hain,
D. Hasell, H. Heßling, Y. Iga, K. Johnson[12], P. Joos, M. Kasemann, R. Klanner, W. Koch, L. Köpke[13], U. Kötz,
H. Kowalski, J. Labs, A. Ladage, B. Löhr, M. Löwe, D. Lüke, J. Mainusch, O. Mańczak, T. Monteiro[14],
J.S.T. Ng, S. Nickel[15], D. Notz, K. Ohrenberg, M. Roco, M. Rohde, J. Roldán, U. Schneekloth, W. Schulz,
F. Selonke, E. Stiliaris[16], B. Surrow, T. Voß, D. Westphal, G. Wolf, C. Youngman, W. Zeuner, J.F. Zhou[17]
Deutsches Elektronen-Synchrotron DESY, Hamburg, Federal Republic of Germany

H.J. Grabosch, A. Kharchilava, A. Leich, M.C.K. Mattingly, A. Meyer, S. Schlenstedt, N. Wulff
DESY-Zeuthen, Inst. für Hochenergiephysik, Zeuthen, Federal Republic of Germany

G. Barbagli, P. Pelfer
University and INFN, Florence, Italy [f]

G. Anzivino, G. Maccarrone, S. De Pasquale, L. Votano
INFN, Laboratori Nazionali di Frascati, Frascati, Italy [f]

A. Bamberger, S. Eisenhardt, A. Freidhof, S. Söldner-Rembold[18], J. Schroeder[19], T. Trefzger
Fakultät für Physik der Universität Freiburg i.Br., Freiburg i.Br., Federal Republic of Germany [c]

I

N.H. Brook, P.J. Bussey, A.T. Doyle[20], J.I. Fleck[4], D.H. Saxon, M.L. Utley, A.S. Wilson
Dept. of Physics and Astronomy, University of Glasgow, Glasgow, U.K. [o]

A. Dannemann, U. Holm, D. Horstmann, T. Neumann, R. Sinkus, K. Wick
Hamburg University, I. Institute of Exp. Physics, Hamburg, Federal Republic of Germany [c]

E. Badura[21], B.D. Burow[22], L. Hagge, E. Lohrmann, J. Milewski, M. Nakahata[23], N. Pavel, G. Poelz, W. Schott,
F. Zetsche
Hamburg University, II. Institute of Exp. Physics, Hamburg, Federal Republic of Germany [c]

T.C. Bacon, N. Bruemmer, I. Butterworth, E. Gallo, V.L. Harris, B.Y.H. Hung, K.R. Long, D.B. Miller,
P.P.O. Morawitz, A. Prinias, J.K. Sedgbeer, A.F. Whitfield
Imperial College London, High Energy Nuclear Physics Group, London, U.K. [o]

U. Mallik, E. McCliment, M.Z. Wang, S.M. Wang, J.T. Wu
University of Iowa, Physics and Astronomy Dept., Iowa City, USA [p]

P. Cloth, D. Filges
Forschungszentrum Jülich, Institut für Kernphysik, Jülich, Federal Republic of Germany

S.H. An, S.M. Hong, S.W. Nam, S.K. Park, M.H. Suh, S.H. Yon
Korea University, Seoul, Korea [h]

R. Imlay, S. Kartik, H.-J. Kim, R.R. McNeil, W. Metcalf, V.K. Nadendla
Louisiana State University, Dept. of Physics and Astronomy, Baton Rouge, LA, USA [p]

F. Barreiro[24], G. Cases, J.P. Fernandez, R. Graciani, J.M. Hernández, L. Hervás[24], L. Labarga[24], M. Martinez,
J. del Peso, J. Puga, J. Terron, J.F. de Trocóniz
Univer. Autónoma Madrid, Depto de Física Teoríca, Madrid, Spain [n]

G.R. Smith
University of Manitoba, Dept. of Physics, Winnipeg, Manitoba, Canada [a]

F. Corriveau, D.S. Hanna, J. Hartmann, L.W. Hung, J.N. Lim, C.G. Matthews, P.M. Patel,
L.E. Sinclair, D.G. Stairs, M. St.Laurent, R. Ullmann, G. Zacek
McGill University, Dept. of Physics, Montréal, Québec, Canada [a, b]

V. Bashkirov, B.A. Dolgoshein, A. Stifutkin
Moscow Engineering Physics Institute, Mosocw, Russia [l]

G.L. Bashindzhagyan, P.F. Ermolov, L.K. Gladilin, Yu.A. Golubkov, V.D. Kobrin, I.A. Korzhavina, V.A. Kuzmin,
O.Yu. Lukina, A.S. Proskuryakov, A.A. Savin, L.M. Shcheglova, A.N. Solomin,
N.P. Zotov
Moscow State University, Institute of Nuclear Physics, Moscow, Russia [m]

M. Botje, F. Chlebana, A. Dake, J. Engelen, M. de Kamps, P. Kooijman, A. Kruse, H. Tiecke, W. Verkerke,
M. Vreeswijk, L. Wiggers, E. de Wolf, R. van Woudenberg
NIKHEF and University of Amsterdam, Netherlands [i]

D. Acosta, B. Bylsma, L.S. Durkin, K. Honscheid, C. Li, T.Y. Ling, K.W. McLean[25], W.N. Murray, I.H. Park,
T.A. Romanowski[26], R. Seidlein[27]
Ohio State University, Physics Department, Columbus, Ohio, USA [p]

D.S. Bailey, A. Byrne[28], R.J. Cashmore, A.M. Cooper-Sarkar, R.C.E. Devenish, N. Harnew,
M. Lancaster, L. Lindemann[4], J.D. McFall, C. Nath, V.A. Noyes, A. Quadt, J.R. Tickner,
H. Uijterwaal, R. Walczak, D.S. Waters, F.F. Wilson, T. Yip
Department of Physics, University of Oxford, Oxford, U.K. [o]

G. Abbiendi, A. Bertolin, R. Brugnera, R. Carlin, F. Dal Corso, M. De Giorgi, U. Dosselli,
S. Limentani, M. Morandin, M. Posocco, L. Stanco, R. Stroili, C. Voci
Dipartimento di Fisica dell' Universita and INFN, Padova, Italy [f]

II

J. Bulmahn, J.M. Butterworth, R.G. Feild, B.Y. Oh, J.J. Whitmore[29]
Pennsylvania State University, Dept. of Physics, University Park, PA, USA [q]

G. D'Agostini, G. Marini, A. Nigro, E. Tassi
Dipartimento di Fisica, Univ. 'La Sapienza' and INFN, Rome, Italy [f]

J.C. Hart, N.A. McCubbin, K. Prytz, T.P. Shah, T.L. Short
Rutherford Appleton Laboratory, Chilton, Didcot, Oxon, U.K. [o]

E. Barberis, T. Dubbs, C. Heusch, M. Van Hook, W. Lockman, J.T. Rahn, H.F.-W. Sadrozinski, A. Seiden, D.C. Williams
University of California, Santa Cruz, CA, USA [p]

J. Biltzinger, R.J. Seifert, O. Schwarzer, A.H. Walenta, G. Zech
Fachbereich Physik der Universität-Gesamthochschule Siegen, Federal Republic of Germany [c]

H. Abramowicz, G. Briskin, S. Dagan[30], A. Levy[31]
School of Physics,Tel-Aviv University, Tel Aviv, Israel [e]

T. Hasegawa, M. Hazumi, T. Ishii, M. Kuze, S. Mine, Y. Nagasawa, M. Nakao, I. Suzuki, K. Tokushuku, S. Yamada, Y. Yamazaki
Institute for Nuclear Study, University of Tokyo, Tokyo, Japan [g]

M. Chiba, R. Hamatsu, T. Hirose, K. Homma, S. Kitamura, Y. Nakamitsu, K. Yamauchi
Tokyo Metropolitan University, Dept. of Physics, Tokyo, Japan [g]

R. Cirio, M. Costa, M.I. Ferrero, L. Lamberti, S. Maselli, C. Peroni, R. Sacchi, A. Solano, A. Staiano
Universita di Torino, Dipartimento di Fisica Sperimentale and INFN, Torino, Italy [f]

M. Dardo
II Faculty of Sciences, Torino University and INFN - Alessandria, Italy [f]

D.C. Bailey, D. Bandyopadhyay, F. Benard, M. Brkic, M.B. Crombie, D.M. Gingrich[32], G.F. Hartner, K.K. Joo, G.M. Levman, J.F. Martin, R.S. Orr, S. Polenz, C.R. Sampson, R.J. Teuscher
University of Toronto, Dept. of Physics, Toronto, Ont., Canada [a]

C.D. Catterall, T.W. Jones, P.B. Kaziewicz, J.B. Lane, R.L. Saunders, J. Shulman
University College London, Physics and Astronomy Dept., London, U.K. [o]

K. Blankenship, B. Lu, L.W. Mo
Virginia Polytechnic Inst. and State University, Physics Dept., Blacksburg, VA, USA [q]

W. Bogusz, K. Charchuła, J. Ciborowski, J. Gajewski, G. Grzelak, M. Kasprzak, M. Krzyżanowski,
K. Muchorowski, R.J. Nowak, J.M. Pawlak, T. Tymieniecka, A.K. Wróblewski, J.A. Zakrzewski, A.F. Żarnecki
Warsaw University, Institute of Experimental Physics, Warsaw, Poland [j]

M. Adamus
Institute for Nuclear Studies, Warsaw, Poland [j]

Y. Eisenberg[30], U. Karshon[30], D. Revel[30], D. Zer-Zion
Weizmann Institute, Nuclear Physics Dept., Rehovot, Israel [d]

I. Ali, W.F. Badgett, B. Behrens, S. Dasu, C. Fordham, C. Foudas, A. Goussiou, R.J. Loveless, D.D. Reeder, S. Silverstein, W.H. Smith, A. Vaiciulis, M. Wodarczyk
University of Wisconsin, Dept. of Physics, Madison, WI, USA [p]

T. Tsurugai
Meiji Gakuin University, Faculty of General Education, Yokohama, Japan

S. Bhadra, M.L. Cardy, C.-P. Fagerstroem, W.R. Frisken, K.M. Furutani, M. Khakzad, W.B. Schmidke
York University, Dept. of Physics, North York, Ont., Canada [a]

IV

1   Introduction

Electron-proton collisions at HERA have shown evidence for hard processes in diffractive reactions. Both in deep inelastic scattering (DIS) ($Q^2 > 10$ GeV^2, where Q^2 is the virtuality of the exchanged photon) [1, 2, 3] and in photoproduction ($Q^2 \sim 0$) [4, 5], events characterized by a large rapidity gap towards the proton direction have been observed and interpreted as resulting from diffractive scattering [1, 2, 4]. In the DIS regime, hard scattering for this class of events has been revealed through the virtuality of the probing photon [1, 3] and through the observation of jet structure in the final state [2]. In the photoproduction domain, the hard scattering has been identified through jet production [4, 5].

Diffractive processes are generally considered to proceed through the exchange of a colourless object with the quantum numbers of the vacuum, generically called the pomeron ($I\!P$). Although the description of soft diffractive processes in terms of pomeron exchange has been a phenomenological success, the description of the pomeron in terms of a parton structure at first lacked experimental support. On the basis of pp data [6] from the CERN ISR, Ingelman and Schlein [7] suggested that the pomeron may have a partonic structure. The observation of jet production in $p\bar{p}$ collisions with a tagged proton (or antiproton) made by the UA8 Collaboration [8] gave strong evidence for such a structure. Further evidence has been provided by the observations made at HERA [1 − 5], which in addition include the first measurements of the diffractive structure function in DIS [9, 10].

The description of diffractive processes in terms of QCD has remained elusive, in part due to the lack of a sufficiently large momentum transfer on which to base the perturbative expansion. Cross sections for diffractive processes involving large transverse energy jets or leptons in the final state are, however, amenable to perturbative QCD calculations [7, 11 − 17]. Their measurement could answer several questions concerning the structure of the pomeron such as: whether the parton picture is valid for the pomeron and universal parton densities can be defined; what fraction of the pomeron momentum is carried by gluons and what by quarks; and whether a momentum sum rule applies to the pomeron [18].

This paper presents the first measurement of inclusive jet cross sections in photoproduction at centre-of-mass energies ~ 200 GeV with a large rapidity gap. This process is sensitive to both the gluon and quark content of the pomeron. In order to examine the partonic structure of the pomeron, these jet cross sections are compared to predictions from models based on perturbative QCD and Regge phenomenology. The jet cross sections measured in photoproduction, combined with the results on the diffractive structure function in deep inelastic scattering [10], give the first experimental evidence for the gluon content of the pomeron. The result does not depend on the flux of pomerons from the proton nor on the assumption that a momentum sum rule can be defined for the pomeron. The data sample used in this analysis corresponds to an integrated luminosity of 0.55 pb^{-1} and was collected during 1993 with the ZEUS detector at HERA.

2   Experimental setup

2.1   HERA operation

The experiment was performed at the electron-proton collider HERA using the ZEUS detector. During 1993 HERA operated with electrons of energy $E_e = 26.7$ GeV colliding with protons of energy $E_p = 820$ GeV. HERA is designed to run with 210 bunches separated by 96 ns in each of the electron and proton rings. For the 1993 data-taking, 84 bunches were filled for each beam

and an additional 10 electron and 6 proton bunches were left unpaired for background studies. The electron and proton beam currents were typically 10 mA, with instantaneous luminosities of approximately $6 \cdot 10^{29}$ cm^{-2} s^{-1}.

2.2 The ZEUS detector and trigger conditions

ZEUS is a multipurpose magnetic detector. The configuration for the 1993 running period has been described elsewhere [2, 19]. A brief description concentrating on those parts of the detector relevant to this analysis is presented here.

Charged particles are tracked by two concentric cylindrical drift chambers, the vertex detector (VXD) and the central tracking detector (CTD), operating in a magnetic field of 1.43 T provided by a thin superconducting coil. The coil is surrounded by a high-resolution uranium-scintillator calorimeter (CAL) divided into three parts, forward[1] (FCAL) covering the pseudorapidity[2] region[3] $4.3 \geq \eta_d \geq 1.1$, barrel (BCAL) covering the central region $1.1 \geq \eta_d \geq -0.75$ and rear (RCAL) covering the backward region $-0.75 \geq \eta_d \geq -3.8$. The solid angle coverage is 99.7% of 4π. The CAL parts are subdivided into towers which in turn are subdivided longitudinally into electromagnetic (EMC) and hadronic (HAC) sections. The sections are subdivided into cells, each viewed by two photomultiplier tubes. The CAL is compensating, with equal response to hadrons and electrons. Measurements under test beam conditions show that the energy resolution is $\sigma_E/E = 0.18/\sqrt{E}$ (E in GeV) for electrons and $\sigma_E/E = 0.35/\sqrt{E}$ for hadrons [20]. In the analysis presented here, CAL cells with EMC (HAC) energy below 60 MeV (110 MeV) are excluded to minimize the effect of calorimeter noise. This noise is dominated by the uranium activity and has an r.m.s. value below 19 MeV for EMC cells and below 30 MeV for HAC cells. For measuring the luminosity as well as for tagging very small Q^2 processes, two lead-scintillator calorimeters [21], located at 107 m and 35 m downstream from the interaction point in the electron direction, detect the bremsstrahlung photons and the scattered electrons respectively.

Data were collected using a three-level trigger [19]. The first-level trigger (FLT) is built as a deadtime-free pipeline. The FLT for the sample of events analysed in this paper required a logical OR of different conditions on sums of energy in the CAL cells. The average FLT acceptance for the events under study was approximately 90%. The second-level trigger used information from a subset of detector components to differentiate physics events from backgrounds consisting mostly of proton beam gas interactions. The third-level trigger (TLT) used the full event information to apply specific physics selections. For this analysis, the following conditions were required: a) the event has a vertex reconstructed by the tracking chambers (VXD+CTD) with the Z value in the range $|Z| < 75$ cm; b) $E - p_Z \geq 8$ GeV, where E is the total energy as measured by the CAL

$$E = \sum_i E_i,$$

p_Z is the Z-component of the vector

$$\vec{p} = \sum_i E_i \vec{r}_i,$$

---

[1] The ZEUS coordinate system is defined as right-handed with the Z axis pointing in the proton beam direction, hereafter referred to as forward, and the X axis horizontal, pointing towards the centre of HERA.

[2] The pseudorapidity is defined as $-\ln(\tan\frac{\theta}{2})$, where the polar angle θ is taken with respect to the proton beam direction, and is denoted by η_d (η) when the polar angle is measured with respect to the nominal interaction point (the reconstructed vertex of the interaction).

[3] The FCAL has the forward edge at $\eta_{\text{edge}} = 4.3$ with full acceptance for $\eta_d < 3.7$.

the sums run over all CAL cells, E_i is the energy of the calorimeter cell i and $\vec{r}_i$ is a unit vector along the line joining the reconstructed vertex and the geometric centre of the cell i; c) $p_Z/E \leq 0.94$ to reject beam-gas interactions; and d) the total transverse energy as measured by the CAL, excluding the cells whose polar angles are below $10°$, exceeds 12 GeV.

3   Diffractive hard photoproduction

Diffractive hard photoproduction processes in ep collisions are characterized by $Q^2 \approx 0$ and by a final state consisting of a hadronic system X containing one or more jets, the scattered electron and the scattered proton

$$e + p_i \rightarrow e + X + p_f \rightarrow e + (jet + X_r) + p_f \tag{1}$$

where p_i (p_f) denotes the initial (final) state proton and X consists of at least one jet plus the remaining hadronic system (X_r).

The kinematics of this process are described in terms of four variables. Two of them describe the electron-photon vertex and can be taken to be the virtuality of the exchanged photon (Q^2) and the inelasticity variable y defined by

$$y = 1 - \frac{E'_e}{E_e}\frac{1 - \cos\theta'_e}{2}$$

where E'_e denotes the scattered electron energy and θ'_e is the electron scattering angle. The other two variables describe the proton vertex: the fraction of the momentum of the initial proton carried by the scattered proton (x_f), and the square of the momentum transfer (t) between the initial and final state proton. In terms of these variables and at low values of Q^2 and t, the square of the mass of the hadronic system X is given by

$$M_X^2 \approx (1 - x_f)\, y\, s \tag{2}$$

where s is the square of the ep centre-of-mass energy.

Diffractive processes in which the photon dissociates give rise to a large rapidity gap between the hadronic system X and the scattered proton:

$$\Delta y_{GAP} = y_{p_f} - y_{max}^{had} \tag{3}$$

where y_{p_f} is the rapidity of the scattered proton and y_{max}^{had} is the rapidity of the most forward going hadron belonging to the system X. The same signature is expected for double dissociation where the scattered proton is replaced by a low mass baryonic system (N). In this paper, the outgoing proton (or system N) was not observed, and instead of y_{max}^{had} the pseudorapidity (η_{max}^{had}) of the most forward-going hadron in the detector was used.

Two cross sections are presented in this paper. First, the cross section for inclusive jet production is measured as a function of the pseudorapidity of the jet (η^{jet}) (for the definition of the jet variables see section 4) in reaction (1) with the most-forward going hadron at $\eta_{max}^{had} < 1.8$. This corresponds to a rapidity gap of at least 2.5 units measured from the edge of the CAL ($\Delta\eta_{GAP} = \eta_{\text{edge}} - \eta_{max}^{had}$). This cross section is denoted by

$$\frac{d\sigma}{d\eta^{jet}}(\eta_{max}^{had} < 1.8) \tag{4}$$

7

and is measured in the η^{jet} range between -1 and 1. Second, the integrated cross section for inclusive jet production is determined as a function of η^0_{max}

$$\sigma(\eta^{had}_{max} < \eta^0_{max}) = \int_{-1}^{+1} d\eta^{jet} \frac{d\sigma}{d\eta^{jet}}(\eta^{had}_{max} < \eta^0_{max}) \tag{5}$$

and is measured in the range of η^0_{max} between 1 and 2.4. Both measurements include contributions from double dissociation where the large-rapidity-gap requirement is satisfied.

The jet cross sections refer to jets at the hadron level with a cone radius, $R = \sqrt{\Delta\eta^2 + \Delta\phi^2}$, of one unit in pseudorapidity (η) $-$ azimuth (ϕ) space and integrated over the transverse energy of the jet $E_T^{jet} > 8$ GeV. They are given in the kinematic region $Q^2 < 4$ GeV^2 and $0.2 < y < 0.85$. This region corresponds to photoproduction interactions at centre-of-mass energies in the range 130-270 GeV with a median $Q^2 \approx 10^{-3}$ GeV^2.

3.1   Models

The description of diffractive hard processes in terms of QCD is still in an early stage. Two main theoretical approaches have been considered. Both assume that a pomeron ($I\!\!P$) is emitted by the proton. The variable $x_{I\!\!P} \equiv 1 - x_f$ is then the fraction of the initial proton's momentum carried by the pomeron and $M_X^2 \approx x_{I\!\!P} y s$ is the square of the $\gamma I\!\!P$ centre-of-mass energy. The two approaches differ in the modelling of jet production in $\gamma I\!\!P$ collisions. One of them [7, 11 $-$ 13] assumes factorisation (factorisable models) while the other one does not [14, 16] (non-factorisable models). The latter are, however, not considered in what follows due to the lack of a Monte Carlo generator with an appropriate description of the event jet structure.

Calculations based on factorisable models involve three basic ingredients: the flux of pomerons from the proton as a function of $x_{I\!\!P}$ and t, the parton densities in the pomeron and the matrix elements for jet production. The pomeron is assumed to be a source of partons which interact either with the photon (direct component) or with a partonic constituent of the photon (resolved component). As an example, the contribution of the direct component to the cross section for reaction (1) is given by

$$\sigma_{dir} = \int dy f_{\gamma/e}(y) \int \int dx_{I\!\!P} dt f_{I\!\!P/p}(x_{I\!\!P}, t) \sum_i \int d\beta \sum_{j,k} \int d\hat{p}_T^2 \frac{d\hat{\sigma}_{i+\gamma \to j+k}}{d\hat{p}_T^2}(\hat{s}, \hat{p}_T^2, \mu^2) \; f_{i/I\!\!P}(\beta, \mu^2) \tag{6}$$

where $f_{\gamma/e}$ is the flux of photons from the electron[4] and $f_{I\!\!P/p}$ is the flux of pomerons from the proton. The sum in i runs over all possible types of partons present in the pomeron, and $f_{i/I\!\!P}(\beta, \mu^2)$ is the density of partons of type i carrying a fraction β of the pomeron momentum at a scale μ^2 and is assumed to be independent of t. The sum in j and k runs over all possible types of final state partons and $\hat{\sigma}_{i+\gamma \to j+k}$ is the cross section for the two-body collision $i + \gamma \to j + k$ and depends on the square of the centre-of-mass energy ($\hat{s}$), the transverse momentum of the two outgoing partons ($\hat{p}_T$) and the momentum scale (μ) at which the strong coupling constant ($\alpha_s(\mu^2)$) is evaluated. One possible choice is $\mu^2 = \hat{p}_T^2$. In these models, the pomeron flux factor is extracted from hadron-hadron collisions using Regge theory, and the matrix elements are computed in perturbative QCD. However, the parton densities in the pomeron have to be extracted from experiment. While the recent measurements of the diffractive structure function in DIS at HERA [9, 10] give information on the quark densities in the pomeron, the gluon content has so far not been determined.

---

[4]The Q^2 dependence has been integrated out using the Weizsäcker-Williams approximation.

Two forms of the pomeron flux factor are commonly used. The Ingelman-Schlein form (IS) [22] uses a parametrisation of UA4 data [23]:

$$f_{I\!P/p}(x_{I\!P}, t) = \frac{c_0}{x_{I\!P}} \cdot (3.19e^{8t} + 0.212e^{3t}) \tag{7}$$

where $c_0 = \frac{1}{2.3}$ GeV^{-2} and t is in GeV^2. The Donnachie-Landshoff form (DL) [12] is calculated in Regge theory, with parameters determined by fits to hadron-hadron data:

$$f_{I\!P/p}(x_{I\!P}, t) = \frac{9b_0^2}{4\pi^2} F_1(t)^2 x_{I\!P}^{1-2\alpha(t)} \tag{8}$$

using the elastic form factor $F_1(t)$ of the proton, the pomeron-quark coupling $b_0 \simeq 1.8$ GeV^{-1} and the pomeron trajectory $\alpha(t) = 1.085 + 0.25t$ with t in GeV^2.

Various parametrisations of the parton densities in the pomeron have been suggested on theoretical grounds [7, 11 − 13]. The following represent extreme possibilities for the shape of the quark and gluon momentum densities:

- hard gluon density $\beta f_{g/I\!P}(\beta, \mu^2) = 6\beta(1-\beta)$;

- soft gluon density $\beta f_{g/I\!P}(\beta, \mu^2) = 6(1-\beta)^5$;

- hard quark density (for two flavours) $\beta f_{q/I\!P}(\beta, \mu^2) = \frac{6}{4}\beta(1-\beta)$.

The first two assume a pomeron made entirely of gluons and the last one a pomeron made of $u\bar{u}$ and $d\bar{d}$ pairs. In all cases a possible μ^2 dependence of the parton densities is neglected[5] and the densities are normalised such that all of the pomeron's momentum is carried by the partons under consideration, $\Sigma_{I\!P}(\mu^2) \equiv \int_0^1 d\beta \sum_i \beta f_{i/I\!P}(\beta, \mu^2) = 1$.

However, since the pomeron is not a particle, it is unclear whether or not the normalisations of the pomeron flux factor and the momentum sum of the pomeron can be defined independently. Nevertheless, for an assumed normalisation of the flux factor, the momentum sum $\Sigma_{I\!P}(\mu^2)$ can be measured. The definition used for the DL form of the pomeron flux factor is the appropriate one if the pomeron were an ordinary hadron and, hence, the one in which the momentum sum rule might be fulfilled [24].

Factorisable models presently account only for diffractive hard processes in which the proton remains intact. Since the measurements are based on the requirement of a large rapidity gap in the central detector, the contribution to the measured cross sections from double dissociation has to be taken into account when comparing with model predictions.

4   Data selection and jet search

Events from quasi-real photon proton collisions were selected using the same criteria as reported earlier [25]. The main steps are briefly discussed here.

Events satisfying the TLT selection described in section 2.2 are first selected. A cone algorithm in η-ϕ space with a cone radius of 1 unit [26, 27] is then used to reconstruct jets, for both data and simulated events (see next section) from the energy deposits in the CAL cells (*cal* jets), and for simulated events also from the final state hadrons (*had* jets). The axis of the jet is

---

[5]The μ^2 dependence of the parton densities in the pomeron is expected to be smaller than the differences between the various parton densities considered [7].

defined according to the Snowmass convention [27], η^{jet} (ϕ^{jet}) is the transverse energy weighted mean pseudorapidity (azimuth) of all the objects (CAL cells or final state hadrons) belonging to that jet. This procedure is explained in detail elsewhere [25]. The variables associated with the *cal* jets are denoted by $E_{T,cal}^{jet}$, η_{cal}^{jet}, and ϕ_{cal}^{jet}, while the ones for the *had* jets by E_T^{jet}, η^{jet}, and ϕ^{jet}.

A search for jet structure using the CAL cells is performed in the data. Events with at least one jet fulfilling the conditions $E_{T,cal}^{jet} > 6$ GeV and $-1 < \eta_{cal}^{jet} < 2$ are retained. Beam-gas interactions, cosmic-ray showers, halo muons and DIS neutral current events are removed from the sample as described previously [25]. The sample thus consists of events from ep interactions with $Q^2 < 4$ GeV^2 and a median $Q^2 \approx 10^{-3}$ GeV^2. The γp centre-of-mass energy (W) is calculated using the expression $W = \sqrt{ys}$. The event sample is restricted to the kinematic range $0.2 < y < 0.85$ using the following procedure. The method of Jacquet-Blondel [28] is used to estimate y from the energies measured in the CAL cells (see section 2.2)

$$y_{JB} = \frac{E - p_Z}{2E_e}.$$

As can be verified using photoproduction events with an electron detected in the luminosity monitor (tagged events), y_{JB} systematically underestimates y by approximately 20%, which is adequately reproduced in the Monte Carlo simulation of the detector. To allow for this effect, the event selection required $0.16 < y_{JB} < 0.7$. The sample thus obtained consists of 19,485 events containing 24,504 jets. The only significant background, which is from misidentified DIS neutral current interactions with $Q^2 > 4$ GeV^2, is estimated to be below 2%. The photoproduction origin of the sample is verified by the expected contribution (26%) of tagged events.

5 Monte Carlo simulation

Events from diffractive hard photoproduction processes were simulated using the program POMPYT [22]. These events were used to determine both the response of the detector to the hadronic final state and the correction factors for the cross sections for jet production with a large rapidity gap.

The POMPYT generator is a Monte Carlo implementation of the model proposed in [7]. The generator makes use of the program PYTHIA [29] to simulate electron-pomeron interactions via resolved and direct photon processes. In PYTHIA, the lepton-photon vertex is modelled according to the Weizsäcker-Williams approximation and the effects of initial state bremsstrahlung from the electron are simulated by using the next-to-leading order electron structure function [30]. Radiative corrections in our kinematic region, where W is larger than 100 GeV, are expected to be negligible [31]. For the resolved processes, the parton densities of the photon were parametrised according to GS-HO [32] and evaluated at the momentum scale set by the transverse momentum of the two outgoing partons, $\mu^2 = \hat{p}_T^2$. The parton densities in the pomeron were parametrised according to the forms described in section 3.1 and were taken to be independent of any scale. In PYTHIA, the partonic processes are simulated using leading order matrix elements, with the inclusion of initial and final state parton showers. Fragmentation into hadrons was performed using the Lund string model [33] as implemented in JETSET [34]. Samples of events were generated with different values of the minimum cutoff for the transverse momentum of the two outgoing partons, starting at $\hat{p}_{Tmin} = 3$ GeV.

The program PYTHIA was also used to simulate standard (non-diffractive) hard photo-production events via resolved and direct photon processes. Events were generated using the leading order predictions of GRV [35] for the photon parton densities and MRSD_ [36] for the proton parton densities.

All generated events were passed through the ZEUS detector and trigger simulation programs. They were reconstructed using the same standard ZEUS off-line programs as for the data.

6   Event characteristics

The event variable η_{max}, as in previous studies by ZEUS [1, 2, 4, 10], was used to select events with a large rapidity gap. For the data, this variable is defined as the pseudorapidity (η_{max}^{cal}) of the most forward condensate with an energy above 400 MeV. A condensate is a contiguous energy deposit above 100 MeV for pure EMC and 200 MeV for HAC or mixed energy deposits in CAL. In the samples of simulated events, the η_{max} variable is defined at both the hadron and CAL levels. At the hadron level, all particles with lifetimes larger than 10^{-13} s, energies in excess of 400 MeV and pseudorapidities below 4.5 are considered as candidates for the most forward final state particle, and η_{max}^{had} defines the pseudorapidity of the most forward particle. The CAL level uses the same definition as for the data.

The mass of the hadronic system (M_X) of each event is reconstructed using the CAL cells, $M_X^{cal} = \sqrt{E^2 - \vec{p}^2}$ [4]. The correlation between M_X^{cal} and η_{max}^{cal} for the sample of events with at least one cal jet fulfilling the conditions $E_{T,cal}^{jet} > 6$ GeV and $-1 < \eta_{cal}^{jet} < 1$ is displayed in Fig. 1a. As shown in our previous publication [4], there exists a distinct class of events with low η_{max}^{cal} values. The large-rapidity-gap events ($\eta_{max}^{cal} < 1.8$) are found to populate the region of low M_X^{cal} values, in contrast to the bulk of the data which have large M_X^{cal} values. These features of the data are reproduced by the Monte Carlo simulations: the events from a simulation of standard hard photoproduction processes using PYTHIA populate the region of large η_{max}^{cal} and large M_X^{cal} values; the events from a simulation of diffractive hard processes using POMPYT extend into the region of low η_{max}^{cal} and M_X^{cal} values.

A study of the region of low M_X^{cal} in the data sample reveals the following features. The η_{max}^{cal} distribution for events with $M_X^{cal} < 30$ GeV is shown in Fig. 1b along with the predictions of PYTHIA and of POMPYT with a pomeron made of hard gluons (normalised to the number of data events above and below $\eta_{max}^{cal} = 2.5$, respectively). The simulation of non-diffractive processes by PYTHIA cannot reproduce the shape of the measured η_{max}^{cal} distribution. On the other hand, the predictions of POMPYT describe well the shape of the data below $\eta_{max}^{cal} \sim 3$.

The M_X^{cal} distribution for the sample of events with $\eta_{max}^{cal} < 1.8$ is shown in Fig. 1c. This sample consists of 49 events containing 68 jets. The data exhibit an enhancement at low masses, 15 GeV $\stackrel{<}{\sim} M_X^{cal} \stackrel{<}{\sim} 30$ GeV, which is reproduced by the simulation of POMPYT with a hard gluon density (normalised to the number of data events). The W of each event is reconstructed using y_{JB}, $W^{cal} = \sqrt{y_{JB}s}$. The distribution of W^{cal} for events with $\eta_{max}^{cal} < 1.8$ is shown in Fig. 1d along with the expectations of POMPYT with a hard gluon density (normalised to the number of data events). The W^{cal} dependence exhibited by the data sample is well reproduced by the simulation of POMPYT. The expectations of POMPYT using a hard quark density (not shown) also give a good description of the distributions of the data. Note that POMPYT assumes the cross section to be independent of W as expected for diffractive processes mediated by pomeron exchange. The good agreement with the data gives evidence for the diffractive nature of the large-rapidity-gap events.

11

In summary, the data exhibit a different behaviour in the region of low masses of the hadronic system compared to that of high masses. At low masses, the shape of the η_{max}^{cal} distribution in the data sample cannot be accounted for by the simulation of non-diffractive processes as in PYTHIA. On the other hand, the features of the data are described by the predictions of diffractive processes mediated by pomeron exchange as in POMPYT. These facts support the interpretation of these large-rapidity-gap events as being produced by diffractive processes via pomeron exchange. Therefore, the measurements of jet cross sections presented in the next section are compared to the predictions of models based on pomeron exchange. However, without a detected fast proton in the forward direction, the jet cross sections refer to events with a large rapidity gap. These include events with a diffractively scattered proton as well as those with a diffractively dissociated proton with mass less than approximately 4 GeV [10]. In this way, the measurements are presented in a model independent form suitable for comparison with calculations other than those presented here.

6.1 Energy and acceptance corrections

The method to correct the transverse energy of a jet as reconstructed using the CAL cells has been discussed elsewhere [25]. For samples of simulated events, the transverse energy of a jet as measured by the CAL ($E_{T,cal}^{jet}$) was compared to that reconstructed using the final state hadrons (E_T^{jet}). The corrections to the jet transverse energy were constructed as multiplicative factors, $C(E_{T,cal}^{jet}, \eta_{cal}^{jet})$, which, when applied to the E_T of the *cal* jets, give the corrected transverse energies of the jets: $E_T^{jet} = C(E_{T,cal}^{jet}, \eta_{cal}^{jet}) \times E_{T,cal}^{jet}$. The function C corrects for energy losses, and for values $E_{T,cal}^{jet} > 10$ GeV is approximately flat as a function of $E_{T,cal}^{jet}$ and varies between 1.08 and 1.18 depending on η_{cal}^{jet}. For $E_{T,cal}^{jet}$ near threshold, $E_{T,cal}^{jet} \approx 6$ GeV, this correction procedure can give values as large as 1.40. No correction is needed for η^{jet} ($\eta^{jet} \approx \eta_{cal}^{jet}$). The procedure was validated by comparing the momenta of the tracks in the *cal* jet in data and in Monte Carlo simulations. From this comparison it was concluded that the energy scale of the jets is corrected to within $\pm$ 5% [25]. The correction procedure was applied to the data sample of jets with $E_{T,cal}^{jet} > 6$ GeV to select for further study those jets with corrected transverse energies of $E_T^{jet} > 8$ GeV and with the jet pseudorapidity in the range between -1 and 1.

The events generated by POMPYT were used to compute the acceptance correction for the inclusive jet distributions. This correction function takes into account the efficiency of the trigger, the selection criteria and the purity and efficiency of the jet and η_{max}^{had} selection. It also corrects for the migrations in the variable η_{max}^{cal} and yields cross sections for the true rapidity gap defined by η_{max}^{had} and $\eta = 4.5$. After applying the jet transverse energy corrections, the purity was $\sim 40\%$ and the efficiency was $\sim 50\%$. Cross sections were then obtained by applying bin-by-bin corrections to the inclusive jet distributions of the data sample in the variables η^{jet} and η_{max}^{had}. The acceptance correction factors for the inclusive jet cross section $d\sigma/d\eta^{jet}(\eta_{max}^{had} < 1.8)$ ($\sigma(\eta_{max}^{had} < \eta_{max}^0)$) were found to vary between 0.63 and 0.93 (0.59 and 0.84). The dependence of these correction factors on the choice of parametrisations of the parton densities in the pomeron were found to be below $\sim 20\%$, and are taken into account in the systematic uncertainty assigned to the measurements reported in the next section.

7   Results

In this section, first the measured jet cross sections are presented and the uncertanties of the measurements discussed. These results are model-independent. Second, the expectations from non-diffractive processes are found not to account for the measurements. Third, the predictions from diffractive models are compared to the data and estimates of the momentum sum of the pomeron and of the relative contribution of quarks and gluons in the pomeron are extracted using solely the diffractive jet measurements. Fourth, the jet cross sections in photoproduction are combined with the measurements of the DIS diffractive structure function to constrain further the parton content of the pomeron.

7.1   Jet Cross Sections

The results for $d\sigma/d\eta^{jet}(\eta_{max}^{had} < 1.8)$ and $\sigma(\eta_{max}^{had} < \eta_{max}^0)$ are presented in Figs. 2 and 3 and in Tables 1 and 2. The differential cross section is flat as a function of η^{jet}. Since the measured jet cross sections refer to events with a large rapidity gap they include a contribution from double dissociation. The statistical errors of the measurements are indicated as the inner error bars in Figs. 2 and 3. They are $\sim 30\%$ for $d\sigma/d\eta^{jet}(\eta_{max}^{had} < 1.8)$ and constitute the dominant source of uncertainty. For $\sigma(\eta_{max}^{had} < \eta_{max}^0)$ the statistical error increases from 8% to 20% as η_{max}^0 decreases. A detailed study of the systematic uncertainties of the measurements has been carried out [25, 37]. The sources of uncertainty include the dependence on the choice of the parton densities in the pomeron, the simulation of the trigger, the cuts used to select the data, and the absolute energy scale of the *cal* jets [25].

The following systematic uncertainties related to the η_{max}-cut were studied: the η_{max}^{cal} variable in the data and the simulated events was recomputed after removing the CAL cells with $\eta > 3.25$ in order to check the dependence on the detailed simulation of the forward region of the detector, resulting in changes up to 13% for $\sigma(\eta_{max}^{had} < \eta_{max}^0)$ and up to 18% for $d\sigma/d\eta^{jet}(\eta_{max}^{had} < 1.8)$ (except at the most forward data point, where the statistics are small and the change amounts to 37%); the energy threshold in the computation of η_{max}^{cal} for data and simulated events was decreased to 300 MeV, yielding changes up to 11% for $d\sigma/d\eta^{jet}(\eta_{max}^{had} < 1.8)$ and up to 14% for $\sigma(\eta_{max}^{had} < \eta_{max}^0)$ (except at the most backward data point, where the statistics are small and the change amounts to 27%).

The dominant source of systematic error is the absolute energy scale of the *cal* jets, known to within 5%, which results in a 20% error. The systematic uncertainties not associated with the energy scale of the jets were added in quadrature to the statistical errors and are shown as the total error bars. The additional uncertainty due to the energy scale of the jets is shown as a shaded band. The systematic uncertainties have large bin to bin correlations. They are to be understood as a conservative estimate of the error associated with each data point. An additional overall normalisation uncertainty of 3.3% from the luminosity determination is not included.

7.2   Comparison to non-diffractive model predictions

The contribution to the measured cross sections from non-diffractive processes was estimated using PYTHIA including resolved and direct processes. *Had* jets were selected in the generated[6] events using the same jet algorithm as for the data and calculating η_{max}^{had} as explained in section

---

[6]These generated events were analysed at the hadron level.

6. In PYTHIA the occurrence of a rapidity gap is exponentially suppressed and arises from a fluctuation in the pseudorapidity distribution of the final state hadrons. The calculations using MRSD$_-$ [36] for the proton and GRV-HO [35] for the photon parton densities are compared to the measurements in Figs. 2 and 3. The non-diffractive contribution does not reproduce the measurements. For the measured $d\sigma/d\eta^{jet}(\eta^{had}_{max} < 1.8)$ the non-diffractive contribution is close to the data only at the most forward measured point. For the remaining η^{jet} range, the data are a factor between 2 and 7 above the expectations from non-diffractive processes. In the measured $\sigma(\eta^{had}_{max} < \eta^0_{max})$, the non-diffractive contribution as predicted by PYTHIA is smaller than the data by factors between 3 and 9. These comparisons, together with the features of the data shown in the previous section, demonstrate that the measured jet cross sections with a large rapidity gap cannot be accounted for by non-diffractive processes. However, in the discussion below, this non-diffractive contribution will be subtracted from the data.

7.3   Comparison to diffractive model predictions

The measured cross sections are compared to the predictions of the models for diffractive hard scattering mediated by pomeron exchange, as implemented in the POMPYT generator. The predictions have been obtained by selecting had jets in the generated events using the same jet algorithm as for the data and calculating η^{had}_{max} as explained in section 6.

In a first step, the predictions of POMPYT, using the DL flux factor and the parametrisations of the pomeron parton densities suggested theoretically (see section 3.1), and assuming $\Sigma_{I\!P} = 1$, are compared to the measured cross sections in Figs. 2 and 3. For this initial comparison, the contributions from non-diffractive and double dissociation processes have not been taken into account. As mentioned earlier (see section 3.1), the μ^2 dependence of the parton densities has been neglected and, hence, the argument of $\Sigma_{I\!P}(\mu^2)$ is omitted. The scale relevant for the measured jet cross sections is $\mu^2 \sim (E^{jet}_T)^2$. We start by discussing the results for $d\sigma/d\eta^{jet}(\eta^{had}_{max} < 1.8)$. The shape of the predictions of POMPYT using a hard parton density compares well with the measured shape of the cross section. The shape predicted by POMPYT using a soft gluon density does not describe the data. The calculations based on a soft gluon density are smaller than the measurements by factors between 20 and 50. This type of parametrisation was already disfavoured by previous studies [5]. The predictions using a hard quark density are too small by factors between 3 and 10, but those using a hard gluon density reproduce the measurements well. The predictions based on the IS flux factor lead to similar conclusions. For the integrated cross section $\sigma(\eta^{had}_{max} < \eta^0_{max})$, the measured shape is in each case described by the expectations from POMPYT, although the normalisation is incorrect by a factor depending on the model. A soft gluon (hard quark) density yields a prediction which is too small by factors between 30 and 60 (5 and 10). A hard gluon density for the pomeron gives a good description of the data. Based on the samples of events of POMPYT, the measurements are sensitive to β values above approximately 0.3. Therefore, the data is not sensitive to a possible additional contribution due to a soft parton component in the pomeron. The data do not rule out a possible contribution from a super-hard parton component in the pomeron [15 − 17].

In principle, other processes could contribute to jet production with a large rapidity gap. For example, the proton may emit a π^+ (instead of a pomeron), $p_i \rightarrow n_f \pi^+$, and a partonic constituent of the π^+ undergoes a hard interaction with the photon or its constituents. The contribution from this reaction to the data is expected to be small due to the power law decrease, $\sim W^{-4}$, for pion exchange. Monte Carlo calculations using POMPYT confirm these

expectations.

In a second step, the data were compared to the predictions of POMPYT based on a pomeron consisting of both quarks and gluons but without assuming $\Sigma_{I\!\!P} = 1$. In addition, the contribution from non-diffractive processes and from double dissociation to the measured cross sections were taken into account. The non-diffractive contribution as predicted by PYTHIA[7] was subtracted bin by bin from the data. The contribution from double dissociation for large-rapidity-gap events was estimated to be $(15 \pm 10)\%$ [10]. This contribution was assumed to be independent of η^{jet} and was also subtracted from the data. After the above subtractions, the data were compared with the predictions of POMPYT using the DL flux factor and allowing for a mixture of the hard gluon $(6\beta(1-\beta))$ and the hard quark $(\frac{6}{4}\beta(1-\beta))$ densities in the pomeron: a fraction c_g for hard gluons and $c_q = 1 - c_g$ for hard quarks. The overall normalisation of the POMPYT prediction was left as a free parameter: $\Sigma_{I\!\!P}$. For this study, the contribution to the cross sections and to $\Sigma_{I\!\!P}$ from possible soft gluon and soft quark components has been neglected.

For each value of c_g, a one-parameter $(\Sigma_{I\!\!P})$ χ^2-fit to the measured $d\sigma/d\eta^{jet}(\eta^{max}_{had} < 1.8)$ was performed. The results are presented in Fig. 4. The thick solid line represents the value of $\Sigma_{I\!\!P}$ for the minimum of the χ^2-fit for each value of c_g and the shaded band represents the 1 σ range around those minima. For $c_g = 1$ (gluons only) the fit yields $\Sigma_{I\!\!P} = 0.5 \pm 0.2$ with $\chi^2_{min} = 2.3$ for three degrees of freedom, while for $c_g = 0$ (quarks only) the fit yields $\Sigma_{I\!\!P} = 2.5 \pm 0.9$ with $\chi^2_{min} = 2.8$. The momentum sum rule $(\Sigma_{I\!\!P} = 1)$ is approximately satisfied for $0.2 < c_g < 0.6$ (statistical errors only). Note that for this estimate the DL form for the pomeron flux factor was assumed.

This comparison of cross sections for jet production with a large rapidity gap between data and model predictions is subject to the following uncertainties:

- The jet cross sections obtained from the Monte Carlo calculations presented here are leading order calculations. In these calculations, $\alpha_s(\mu^2)$ and the parton densities in the proton and the photon are evaluated at $\mu^2 = \hat{p}^2_T$. These computations may be affected by higher order QCD corrections, which are expected to change mainly the normalisation (K-factor). The agreement between the PYTHIA calculations of the inclusive jet differential cross sections and the measurements [25] indicate that in the case of the non-diffractive contribution the K-factor is close to 1, within an uncertainty of $\sim 20\%$. The K-factor in the case of POMPYT is expected to be similar (with a similar uncertainty), as the same hard subprocesses are involved in the calculation of jet cross sections.

- The amount of the non-diffractive contribution to the measured cross section was modelled using PYTHIA with some choices for the proton and photon parton densities. This contribution is more sensitive to the choice of photon parton densities.

- The uncertainty in the estimation of the contribution from double dissociation.

- The POMPYT model for diffractive hard scattering assumes factorisation of the hard process with respect to the soft diffractive reaction. The extent to which this assumption is valid has to be determined experimentally through a detailed comparison of measurements for different reactions (see next section).

---

[7]These calculations give a good description of the inclusive jet differential cross sections (without the large-rapidity-gap requirement) in the range $-1 < \eta^{jet} < 1$ [25].

- The pomeron flux factors adopted in the various models are based on different assumptions for the t and $x_{I\!\!P}$ dependences which are obtained from data on soft diffractive hadronic processes. The uncertainty in the procedure used to extract the flux is about 30%.

The differences between the results obtained in each of the studies listed above and the central values were combined in quadrature to yield the theoretical systematic uncertainties (not shown in Fig. 4) of the fitted values of $\Sigma_{I\!\!P}$. These uncertainties were then added in quadrature with the statistical and systematic uncertainties of the measurements resulting in the following ranges at the $1\ \sigma$ level: $1.4 < \Sigma_{I\!\!P} < 3.8$ for $c_g = 0$ and $0.3 < \Sigma_{I\!\!P} < 0.9$ for $c_g = 1$. The range in $\Sigma_{I\!\!P}$ assumes the DL convention for the pomeron flux factor. This normalisation has recently been discussed by Landshoff [38] who concludes that the normalisation is arbitrary up to a multiplicative factor A. If the normalisation is changed by a factor A, the range of the momentum sum is given by $1.4/A < \Sigma_{I\!\!P} < 3.8/A$ for $c_g = 0$ and by $0.3/A < \Sigma_{I\!\!P} < 0.9/A$ for $c_g = 1$.

In summary, the comparison of model predictions with the jet cross section measurements favours those models where the partonic content of the pomeron has a hard contribution. Given the uncertainties mentioned above and the DL convention for the normalisation of the pomeron flux factor, the data can be reproduced by a pomeron whose partonic content varies between a pure hard quark density with momentum sum given by $1.4 < \Sigma_{I\!\!P} < 3.8$ and a pure hard gluon density with $0.3 < \Sigma_{I\!\!P} < 0.9$.

7.4 The gluon content of the pomeron

The HERA experiments have recently presented the first measurements of the diffractive structure function in DIS [9, 10]. The results show that the quark densities in the pomeron have a hard and a soft contribution. Assuming the DL form for the pomeron flux factor, the DIS data do not favour a pomeron structure function which simultaneously fulfils the momentum sum rule and consists exclusively of quarks.

If the pomeron parton densities are universal and describe both DIS and photoproduction processes, the DIS results together with the photoproduction data further constrain the partonic content of the pomeron. The measured diffractive structure function in DIS ($F_2^{D(3)}(\beta, Q^2, x_{I\!\!P})$) [9, 10] can be used to extract the contribution of the quarks to the momentum sum ($\Sigma_{I\!\!P q}(Q^2)$). The integral of $F_2^{D(3)}$ over $x_{I\!\!P}$ and β is proportional to $\Sigma_{I\!\!P q}(Q^2)$:

$$\int_{x_{I\!\!P min}}^{x_{I\!\!P max}} dx_{I\!\!P} \int_0^1 d\beta\ F_2^{D(3)}(\beta, Q^2, x_{I\!\!P}) = k_f \cdot \Sigma_{I\!\!P q}(Q^2) \cdot I_{flux} \tag{9}$$

where I_{flux} is the integral of the pomeron flux factor over t and over the same region in $x_{I\!\!P}$, and k_f is a number which depends on the number of flavours assumed (5/18 for two flavours and 2/9 for three flavours). For the left-hand side of Eq. (9), the parametrisation of $F_2^{D(3)}(\beta, Q^2, x_{I\!\!P})$ obtained in [10] was used. The integral was performed over the range $6.3 \cdot 10^{-4} < x_{I\!\!P} < 10^{-2}$ of the ZEUS DIS measurements. The DL form for the pomeron flux factor was used to compute I_{flux} for the right hand side of Eq. (9). This procedure yields an estimate of $\Sigma_{I\!\!P q}(Q^2)$: 0.32 ± 0.05 (0.40 ± 0.07) for two (three) flavours. These estimates are based on a parametrisation of $F_2^{D(3)}(\beta, Q^2, x_{I\!\!P})$ which was determined in the large β region ($0.1 < \beta < 0.8$) and is assumed to be valid for the entire region $0 < \beta < 1$. In the range of Q^2 where the DIS measurements were done, $8\ \mathrm{GeV}^2 < Q^2 < 100\ \mathrm{GeV}^2$, the pomeron structure function is approximately independent of Q^2 and, thus, the estimated $\Sigma_{I\!\!P q}(Q^2)$ does not depend

upon Q^2. It should be noted that the scales at which the parton densities in the pomeron are probed in DIS, Q^2, and in photoproduction, μ^2, are comparable. The estimate from DIS imposes a constraint on the $\Sigma_{I\!P} - c_g$ plane which, combined with the estimates obtained in the preceding section, restricts the allowed ranges for $\Sigma_{I\!P}$ and the relative contributions of quarks and gluons (c_g). The DIS constraint, which can be written as $\Sigma_{I\!P} \cdot (1 - c_g) = 0.32$ (0.40) for the two choices of the number of flavours, is included in Fig. 4 (the dark shaded area represents the uncertainty in this constraint). Combining the estimates from photoproduction (thick solid line) and DIS yields $0.5 < \Sigma_{I\!P} < 1.1$ and $0.35 < c_g < 0.7$ (statistical errors only).

These results are subject to the uncertainties listed at the end of section 7.3. The allowed range for $\Sigma_{I\!P}$ which results from the combination of the DIS and photoproduction measurements was evaluated for each source of systematic uncertainty. Taking into account all the uncertainties mentioned, the comparison between the DIS and photoproduction measurements gives $0.4 < \Sigma_{I\!P} < 1.6$ for the momentum sum of the pomeron assuming the DL convention for the flux. If the normalisation of the pomeron flux factor is changed by a multiplicative factor A, the allowed range of the momentum sum is given by $0.4/A < \Sigma_{I\!P} < 1.6/A$.

It should be noted that the evaluation of the c_g range allowed by the DIS and photoproduction measurements is not affected by the normalisation of the pomeron flux factor or the uncertainty on the double dissociation contribution since they cancel out in the comparison[8]. Taking into account the remaining uncertainties the combination of the DIS and photoproduction data gives $0.3 < c_g < 0.8$. This result does not depend on the validity of the momentum sum rule for the pomeron.

8   Summary and conclusions

Measurements of ep cross sections for inclusive jet photoproduction with a large rapidity gap in ep collisions at $\sqrt{s} = 296$ GeV using data collected by the ZEUS experiment in 1993 have been presented. The measured jet cross sections are compared to perturbative QCD calculations of diffractive hard processes and allow a model dependent determination of the parton content of the pomeron. The measurements require a contribution from a hard momentum density of the partons in the pomeron. This result is consistent with the observations of the UA8 Collaboration made in $p\bar{p}$ collisions. When the measured jet cross sections are combined with the results on the diffractive structure function in deep inelastic scattering at HERA, first experimental evidence for the gluon content of the pomeron is found. This evidence is independent of the normalisation of the flux of pomerons from the proton and does not rely on assumptions on the momentum sum of the pomeron. The data indicate that between 30% and 80% of the momentum of the pomeron carried by partons is due to hard gluons.

---

[8]This cancellation occurs as long as the same pomeron flux factor is used in both DIS and photoproduction.

References

[1] ZEUS Collab., M. Derrick et al., Phys. Lett. B315 (1993) 481.

[2] ZEUS Collab., M. Derrick et al., Phys. Lett. B332 (1994) 228.

[3] H1 Collab., T. Ahmed et al., Nucl. Phys. B429 (1994) 477.

[4] ZEUS Collab., M. Derrick et al., Phys. Lett. B346 (1995) 399.

[5] H1 Collab., T. Ahmed et al., Nucl. Phys. B435 (1995) 3.

[6] R608 Collab., A.M. Smith et al., Phys. Lett. B163 (1985) 267, B167 (1986) 248; T. Henkes et al., Phys. Lett. B283 (1992) 155.

[7] G. Ingelman and P.E. Schlein, Phys. Lett. B152 (1985) 256.

[8] UA8 Collab., A. Brandt et al., Phys. Lett. B211 (1988) 239, B297 (1992) 417.

[9] H1 Collab., T. Ahmed et al., Phys. Lett. B348 (1995) 681.

[10] ZEUS Collab., M. Derrick et al., DESY 95-093.

[11] E.L. Berger et al., Nucl. Phys. B286 (1987) 704.

[12] A. Donnachie and P.V. Landshoff, Nucl. Phys. B303 (1988) 634, Phys. Lett. B285 (1992) 172.

[13] K.H. Streng, Proc. of the HERA Workshop, edited by R.D. Peccei, Hamburg, Germany (DESY, 1987), p. 365.

[14] N.N. Nikolaev and B.G. Zakharov, Z. Phys. C53 (1992) 331; M. Genovese, N.N. Nikolaev and B.G. Zakharov, KFA-IKP(Th)-1994-37 and CERN-TH.13/95.

[15] J.C. Collins et al., Phys. Rev. D51 (1995) 3182.

[16] J.C. Collins, L. Frankfurt and M. Strikman, Phys. Lett. B307 (1993) 161; A. Berera and D.E. Soper, Phys. Rev. D50 (1994) 4328.

[17] B.A. Kniehl, H.-G. Kohrs and G. Kramer, Z. Phys. C65 (1995) 657.

[18] A. Capella et al., Phys. Lett. B343 (1995) 403.

[19] The ZEUS Detector, Status Report (1993), DESY 1993.

[20] A. Andresen et al., Nucl. Inst. Meth. A309 (1991) 101; A. Caldwell et al., Nucl. Inst. Meth. A321 (1992) 356; A. Bernstein et al., Nucl. Inst. and Meth. A336 (1993) 23.

[21] J. Andruszków et al., DESY 92-066 (1992).

[22] P. Bruni and G. Ingelman, Proc. of the International Europhysics Conference, edited by J. Carr and M. Perrotet, Marseille, France, July 1993 (Ed. Frontieres, Gif-sur-Yvette, 1994, p. 595).

[23] UA4 Collab., M. Bozzo et al., Phys. Lett. B136 (1984) 217.

[24] A. Donnachie and P.V. Landshoff, Proc. of the HERA Workshop, edited by R.D. Peccei, Hamburg, Germany (DESY, 1987), p. 351.

[25] ZEUS Collab., M. Derrick et al., Phys. Lett. B342 (1995) 417.

[26] UA1 Collab., G. Arnison et al., Phys. Lett. B123 (1983) 115.

[27] J. Huth et al., Proc. of the 1990 DPF Summer Study on High Energy Physics, Snowmass, Colorado, edited by E.L. Berger (World Scientific, Singapore, 1990) p. 134.

[28] Method proposed by F. Jacquet and A. Blondel in Proc. of the Study for an ep Facility for Europe, U. Amaldi et al., DESY 79/48 (1979) 377; see also G. D'Agostini and D. Monaldi, Z. Phys. C48 (1990) 467; K.J. Abraham et al., Proc. of ECFA Workshop on LHC, Aachen (1990) 899; R. van Woudenberg et al., Proc. of the Workshop on Physics at HERA, edited by W. Buchmüller and G. Ingelman, Hamburg, Germany (DESY, 1991), p. 739.

[29] H.-U. Bengtsson and T. Sjöstrand, Comp. Phys. Comm. 46 (1987) 43 and T. Sjöstrand, CERN-TH.6488/92.

[30] R. Kleiss et al., in 'Z Physics at LEP 1', eds. G. Altarelli, R. Kleiss and C. Verzegnassi, CERN-89-08, Vol. 3, p.1.

[31] ZEUS Collab., M. Derrick et al., Phys. Lett. B293 (1992) 465.

[32] L.E. Gordon and J.K. Storrow, Z. Phys. C56 (1992) 307.

[33] B. Andersson et al., Phys. Rep. 97 (1983) 31.

[34] T. Sjöstrand, Comp. Phys. Comm. 39 (1986) 347; T. Sjöstrand and M. Bengtsson, Comp. Phys. Comm. 43 (1987) 367.

[35] M. Glück, E. Reya and A. Vogt, Phys. Rev. D46 (1992) 1973.

[36] A.D. Martin, W.J. Stirling and R.G. Roberts, Phys. Rev. D47 (1993) 867.

[37] K. Desch, Ph.D. Thesis, Physikalisches Institut der Universität Bonn (1994).

[38] P.V. Landshoff, HEP-PH-9505254, talk given at the Workshop on Deep Inelastic Scattering and QCD (DIS 95), Paris, France, 24-28 April 1995 and at the 10th Workshop on Photon-Photon Collisions (PHOTON '95), Sheffield, England, 8-13 April 1995.

η^{jet} range	$d\sigma/d\eta^{jet}(\eta^{had}_{max} < 1.8)\pm$stat.$\pm$syst.$\pm$syst. E^{jet}_T-scale (in pb)
(-1,-0.5)	$44 \pm 12 \pm 8\ ^{+10}_{-8}$
(-0.5,0)	$39 \pm 11 \pm 5\ ^{+8}_{-5}$
(0,0.5)	$37 \pm 10 \pm 10\ ^{+8}_{-6}$
(0.5,1)	$16 \pm 6 \pm 7\ ^{+3}_{-3}$

Table 1: Measured differential ep cross section $d\sigma/d\eta^{jet}(\eta^{had}_{max} < 1.8)$ for inclusive jet production for $E^{jet}_T > 8$ GeV and in the kinematic region $Q^2 \leq 4$ GeV^2 and $0.2 < y < 0.85$. The η^{jet} ranges used for the measurements are shown. The cross sections are given at the centre of each η^{jet} bin. The statistical and systematic errors are also indicated. The systematic uncertainties associated with the energy scale of the jets are quoted separately. The overall normalisation uncertainty of 3.3% is not included.

η^0_{max}	$\sigma(\eta_{max} < \eta^0_{max})\pm$stat.$\pm$syst.$\pm$syst. E^{jet}_T-scale (in pb)
1.0	$27.3 \pm 5.5 \pm 9.9\ ^{+5.9}_{-4.5}$
1.5	$51.7 \pm 8.5 \pm 9.2\ ^{+10.7}_{-9.1}$
1.8	$67 \pm 10 \pm 12\ ^{+13}_{-11}$
2.0	$98 \pm 12 \pm 14\ ^{+20}_{-17}$
2.2	$145 \pm 15 \pm 29\ ^{+30}_{-23}$
2.4	$208 \pm 18 \pm 43\ ^{+40}_{-34}$

Table 2: Measured integrated ep cross section $\sigma(\eta^{had}_{max} < \eta^0_{max})$ for inclusive jet production for $E^{jet}_T > 8$ GeV and $-1 < \eta^{jet} < 1$ in the kinematic region $Q^2 \leq 4$ GeV^2 and $0.2 < y < 0.85$. The statistical and systematic errors are also indicated. The systematic uncertainties associated with the energy scale of the jets are quoted separately. The overall normalisation uncertainty of 3.3% is not included.
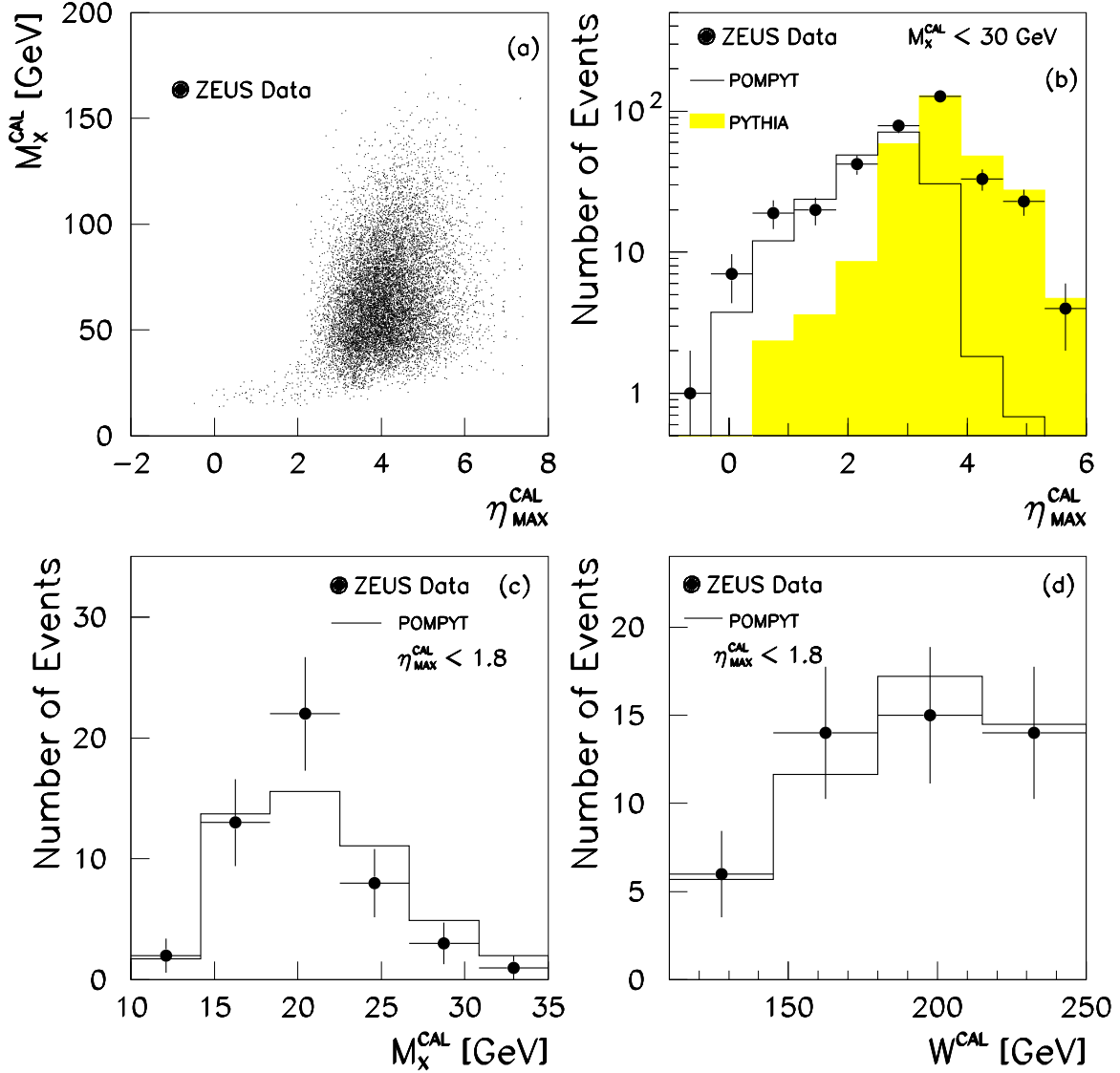
Figure 1: (a) The scatter plot of M_X^{cal} versus η_{max}^{cal} for the sample of events with at least one *cal* jet fulfilling the conditions $E_{T,cal}^{jet} > 6$ GeV and $-1 < \eta_{cal}^{jet} < 1$; (b) the distribution of η_{max}^{cal} for the events with $M_X^{cal} < 30$ GeV along with the predictions of PYTHIA (shaded area) and POMPYT with a hard gluon density in the pomeron (solid line). The predictions are normalised to the number of data events above and below $\eta_{max}^{cal} = 2.5$, respectively; (c) the distribution in M_X^{cal} for the events with $\eta_{max}^{cal} < 1.8$ together with the prediction of POMPYT with a hard gluon density in the pomeron (solid line) normalised to the number of data events; (d) the distribution in W^{cal} for the events with $\eta_{max}^{cal} < 1.8$ and the prediction of POMPYT as in (c).
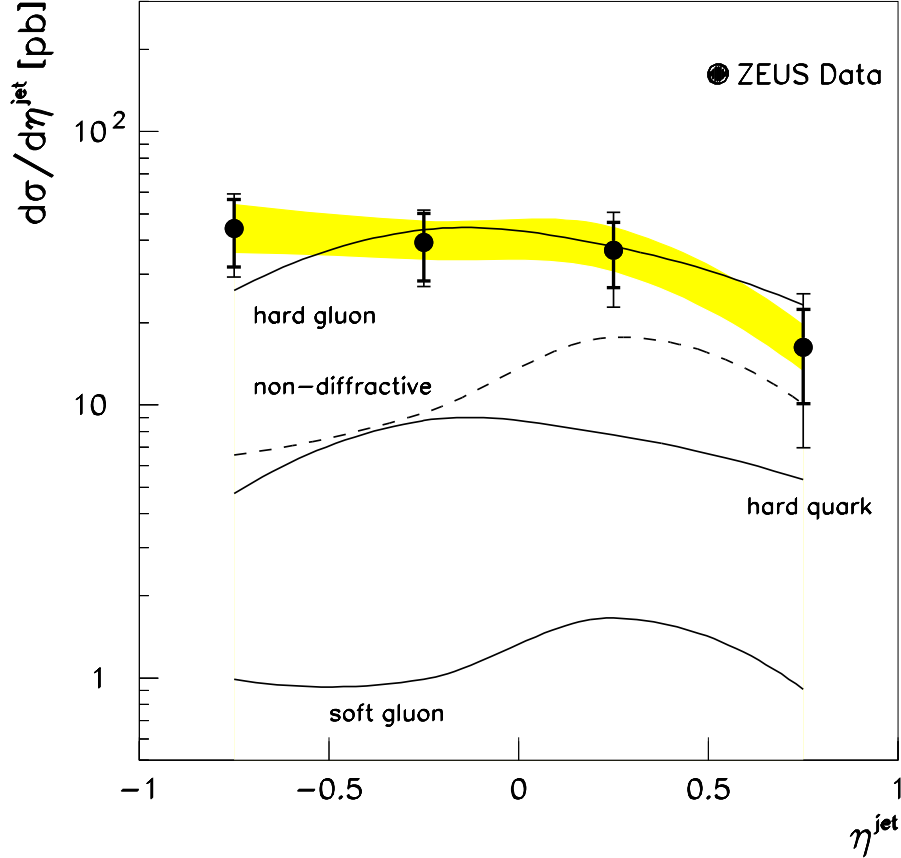
Figure 2: Measured differential ep cross section $d\sigma/d\eta^{jet}(\eta^{had}_{max} < 1.8)$ for inclusive jet production for $E^{jet}_T > 8$ GeV in the kinematic region $Q^2 \le 4$ GeV^2 and $0.2 < y < 0.85$ (dots). The measurements are not corrected for the contributions from non-diffractive processes and double dissociation. The inner error bars represent the statistical errors of the data, and the total error bars show the statistical and systematic errors −not associated with the energy scale of the jets− added in quadrature. The shaded band displays the uncertainty due to the energy scale of the jets. For comparison, POMPYT predictions for single diffractive jet production $(e+p \rightarrow e+p+jet+X_r)$ using the DL flux factor for direct plus resolved processes for various parametrisations of the pomeron parton densities (hard gluon, upper solid line; hard quark, middle solid line; soft gluon, lower solid line) are also shown. The GS-HO photon parton densities have been used in POMPYT. The contribution from non-diffractive processes is exemplified by the PYTHIA predictions using MRSD_ (GRV-HO) for the proton (photon) parton densities (dashed line).
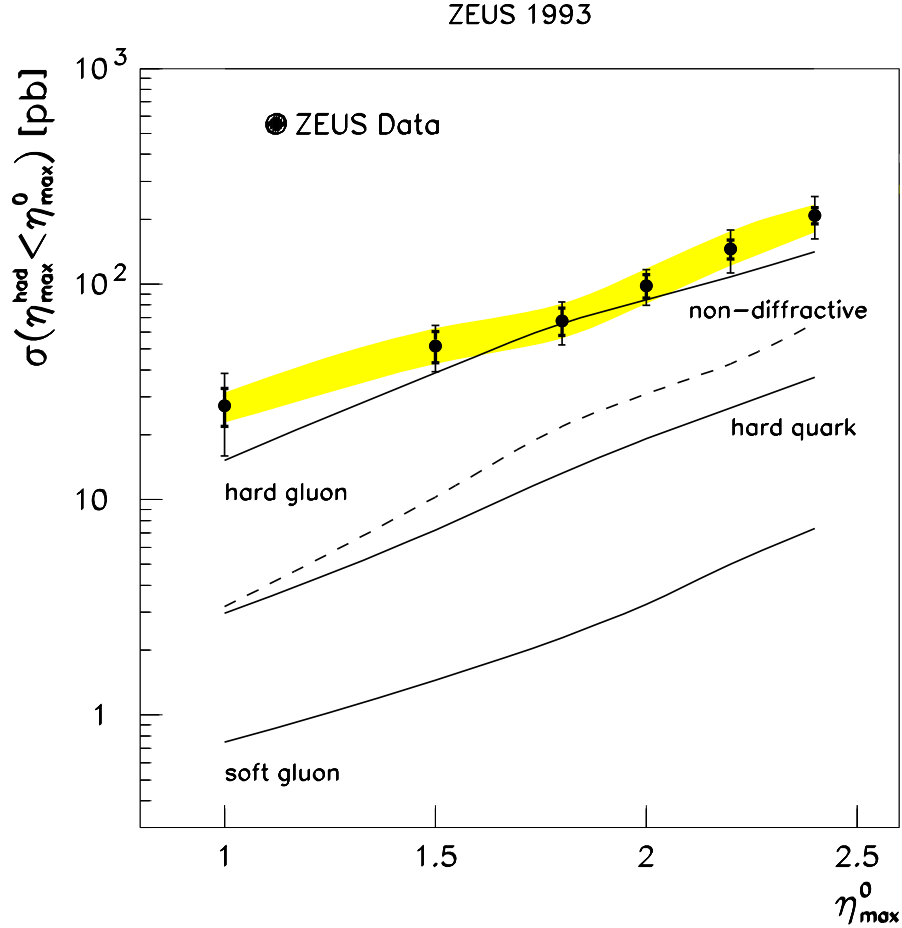
Figure 3: Measured integrated ep cross section $\sigma(\eta_{max}^{had} < \eta_{max}^0)$ for inclusive jet production for $-1 < \eta^{jet} < 1$ and $E_T^{jet} > 8$ GeV in the kinematic region $Q^2 \leq 4$ GeV^2 and $0.2 < y < 0.85$ (dots). The measurements are not corrected for the contributions from non-diffractive processes and double dissociation. The inner error bars represent the statistical errors of the data, and the total error bars show the statistical and systematic errors −not associated with the energy scale of the jets− added in quadrature. The shaded band displays the uncertainty due to the energy scale of the jets. For comparison, PYTHIA and POMPYT calculations (for the same conditions as in Fig. 2) are included.
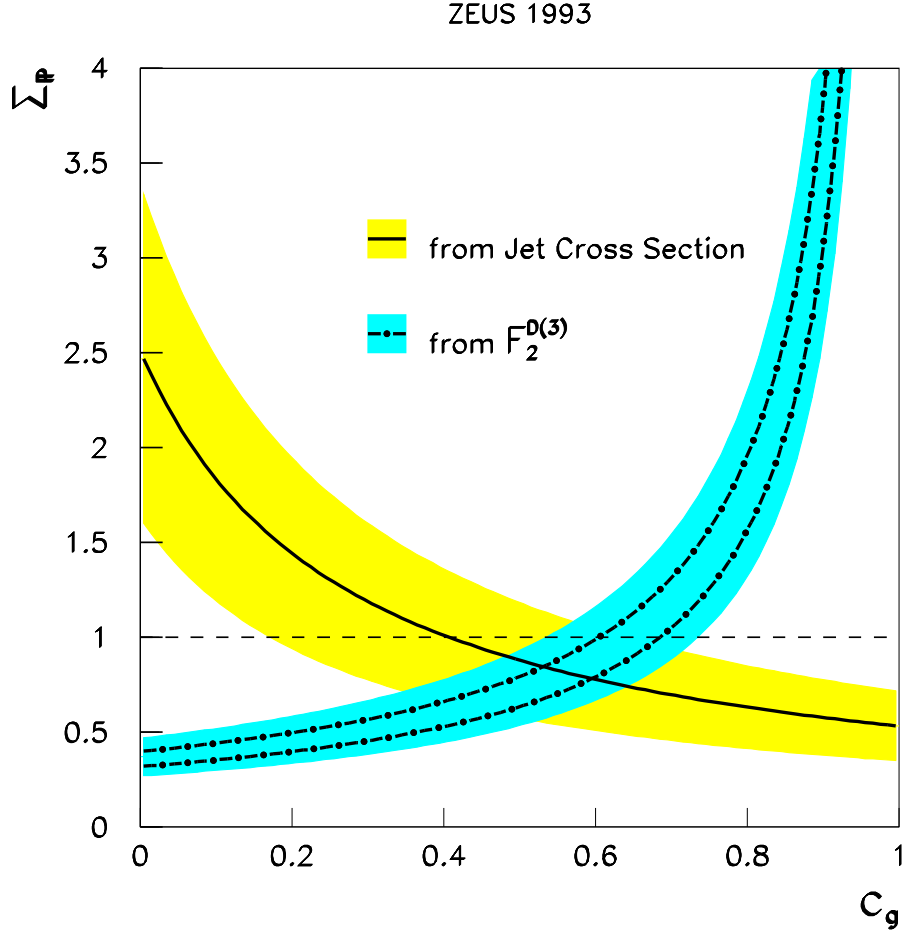
Figure 4: The plane of the variables $\Sigma_{I\!\!P}$ (momentum sum) and c_g (relative contribution of hard gluons in the pomeron). The thick solid line displays the minimum for each value of c_g obtained from the χ^2 fit (the shaded area represents the 1 σ band around these minima) to the measured $d\sigma/d\eta^{jet}(\eta_{max}^{had} < 1.8)$ using the predictions of POMPYT. The constraint imposed in the $\Sigma_{I\!\!P} - c_g$ plane by the measurement of the diffractive structure function in DIS ($F_2^{D(3)}$) [10] for two choices of the number of flavours (upper dot-dashed line for $\Sigma_{I\!\!P\,q} = 0.40$ and lower dot-dashed line for $\Sigma_{I\!\!P\,q} = 0.32$) is also shown. The horizontal dashed line displays the relation $\Sigma_{I\!\!P} = 1$.